Determination of Convective Heat Transfer for Fenestration with Between-the-Glass Louvered Shades

Mike Collins Syeda Tasnim John Wright
Department of Mechanical Engineering
University of Waterloo
Waterloo, Ontario, Canada

ABSTRACT

In previous work, a two-dimensional steady laminar natural convection model of a window cavity with between-panes louvers (i.e., slats) was developed by approximating the system as a vertical cavity with isothermal walls at different temperatures, and with rotatable baffles located midway between the walls. The baffles were set to a third temperature so that night-time and day-time conditions, and the effects of low emissivity coatings (low-e), could be considered. It was found that the system is suited to a traditional one-dimensional analysis. A novel approach that allows the use of standard vertical cavity convection correlations and a modified cavity half-width is described, and a cavity modification factor, n^*, is presented. Finally, the n^* factor and vertical cavity convection correlation are joined with a longwave radiant model, and the results are compared to experimental results. The models show good agreement with experiments.

NOMENCLATURE

Symbols

C_p	Specific heat, J/kgK
g	Gravity, m^2/s
h	Heat transfer coef., W/m^2K
H	Cavity height, mm
k	Conductivity, W/mK
n^*	Cavity modification factor
Nu	Nusselt number, dim
p	Pressure, Pa
P	Louver pitch, mm
Pr	Prandtl number, dim
q''	Heat flux, W/m^2
R	Thermal resistance, m^2K/W

Ra	Rayleigh number, dim
T	Temperature, ◦C, K
U	Thermal transmissivity, W/m^{2}K
w	Louver width, mm
W	Cavity width, mm

Greek Symbols

α	Thermal diffusivity, m^2/s
Δ	change/difference
ϕ	Louver angle, deg
ρ	Density, kg/m^3
μ	Viscosity, kg/ms
Θ	Temperature, dim

Subscripts

c	Convection
cg	Centre-Glass
glass	Glass
local	Local
r	Radiation
ref	Reference
1	Left Wall/Left Glass
2	Right Wall/Right Glass
3	Louver/Baffle

Superscripts

'	Modified half-cavity

INTRODUCTION

The objective of this paper is to develop a correlation that predicts the natural convection heat transfer in window cavities containing rotatable louvered shades. Such systems have become increasingly popular, and accurate heat transfer correlations are required for rating purposes and building energy analysis. Such systems have been

examined extensively in recent times. To date, however, none have looked at the situation where the system is sunlit.

Garnet [1] measured the centre glass heat transfer of a window system with an aluminum louvered blind between two panes of glass. Experiments were run at several different blind louver angles and three different pane spacings. It was observed that, for the blind in the fully open position, the presence of the blind decreased the window's thermal resistance. It was speculated that while in this position, conduction effects in the blinds was having a significant effect. For all cavity widths a steady improvement in the performance of the window was observed as the blind was closed.

Yahoda [2] and Yahoda and Wright [3,4] performed detailed modelling of the effective longwave radiative and solar/optical properties of a louvered blind layer that could be placed anywhere in the window system. The effective longwave radiative properties model was were based on fundamental radiant exchange analysis, and accounted for the louver width, spacing, angle of tilt, and emissivity. The effective solar-optical properties model treated solar beam and diffuse radiation separately. Finally, a simplified center-glass model of thermal transmissivity (*U*-factor) was proposed by combining the longwave radiation model with some simple convection correlations. This model was moderately successful.

Naylor and Collins [5] developed a two-dimensional numerical model of the conjugate convection, conduction and radiative heat transfer in a double glazed window with a between-panes louvered blind. They obtained numerical results both with and without the effects of thermal radiation. It was concluded that data from a conjugate convection-conduction CFD model can be subsequently combined with a very simple radiation model to estimate the *U*-factor of the complete window/blind enclosure.

Recently, Huang [6] conducted an experimental investigation similar to that of Garnet [2]. He examined the effects of louvers on the convective and radiative heat transfer inside a vertical window cavity using two sets of glazings; clear/clear and low-e/clear. His experiment used isothermal vertical surfaces at various pane spacings and louver angles to examine the centre-glass *U*-factor. The results showed better window performance when the louvers were tilted from their fully open position and also when the low-e coating was used. A simplified convective heat transfer model was developed which was subsequently combined with Yahoda's [2] longwave radiation model to predict the centre-glass *U*-factor. The new model reproduced experimental data accurately.

In this study, natural convection heat transfer was studied numerically and a correlation was developed that predicts convective heat transfer in the cavity. Convective heat transfer was considered for situations when the blind was at a third prescribed temperature relative to the glass temperatures. As a 3-temperaure analysis, simulation of heat transfer can be performed for cases where the shade is hotter than the glass; simulating absorbed solar radiation. That is, the system was analyzed for situations that represent sunlit conditions. Full details of the numerical model are provided in Tasnim et al. [7]. The correlation has been coupled with Yahoda's [2] longwave model, and comparisons were made to the results of Huang [6].

It is noted that the present approach is intended eventually fit with the established methodology that is currently employed by window modeling and building analysis software. The various modes of heat transfer are coupled via an energy balance through a one-dimensional model of the center-glass region of the system. Many of the assumptions made in the present work are motivated by this methodology.

NUMERICAL MODEL

In the numerical model, a tall vertical enclosure was chosen to represent the glazing cavity, and baffles located on the vertical centre line of the enclosure represented the blind louvers (Figure 1). The two window panes (AB and CD) were set apart at a distance, W, and a height, H, and were assumed to be isothermal. The end walls (BC and DA) were assumed to be adiabatic. The blind consisted of a set of evenly spaced isothermal baffles of width, w, and pitch, P, (pitch is the vertical distance between two consecutive louvers), which could be rotated about their centre to an angle, ϕ, from the horizontal. The baffles were assumed to be made of a material with high thermal conductivity, and flat with zero thickness.

Three temperatures were required to model the system. In this study, T_1 and T_2 are the left wall (AB) and right wall (CD) temperatures, and T_3 is the baffle temperature. For convenience, the temperature difference across the cavity and dimensionless baffle temperature are defined as $\Delta T=T_2-T_1$ and $\Theta_3=(T_3-T_1)/(T_2-T_1)$, respectively. Air properties were evaluated at a reference temperature, $T_{ref.}$, that represents all three temperatures in the system with the baffle temperature predominating.

$$T_{ref} = \frac{1}{2}\left(\frac{T_1 + T_2}{2} + T_3\right) \tag{1}$$

The air properties at T_{ref} were taken from Hilsenrath [8].

The numerical model was an approximation of a real fenestration. For an actual window, there would be frame effects and only the center-glass region would be nearly isothermal. The idealized system was, however, consistent with the experimental setup used in the examination conducted by Huang [6]. Geometric parameters that remained constant for all numerical simulations are given in Table 1.

To understand the flow field and heat transfer characteristics of the system, a matrix of three different wall spacings (W=17.8 mm, 25.4 mm, and 40.0 mm), three different wall-to-wall temperatures (ΔT=35^{o}C, 10 ^{o}C, and -15 ^{o}C), three different baffle temperatures (Θ_3= 0, 0.5, and 1), and three different baffle angles (ϕ=0^{o}, 45^{o}, and -45^{o}) were considered. Some additional baffle temperatures were also included for W=17.8 mm and 25.4 mm to account for significant solar input to the shade layer. Table 2 presents the matrix of conditions considered in this study.

Steady laminar natural convective heat transfer in the system is described by the fundamental conservation laws of mass, momentum, and energy. The Boussinesq approximation was applied to the y-momentum equation, and the assumptions of an incompressible fluid flow with negligible viscous dissipation, and constant thermo-physical properties was made. No slip conditions were applied to all surfaces, the temperature was specified for both side walls and the baffles, and the end surfaces were adiabatic.

The steady state governing equations were discretized by the finite-volume-method using a third order Quick scheme [9]. The solution procedures included the conjugate gradient method and the PISO algorithm (Pressure-Implicit with Splitting of Operations) [10] to ensure correct linkage between pressure and velocity. The typical number of iterations needed to obtain convergence was between 5,000 and 10,000. The tolerance of the normalized residuals upon convergence was set to 10^{-5} for every calculation case.

To provide confidence in the numerical model, grid dependency was examined and steady laminar natural convection in a vertical cavity was also studied numerically, and compared to published solutions. The results of those tests provided confidence in the numerical model.

Complete details of the numerical model development, validation, and production and analysis of results can be found in Tasnim et al. [7].

NUMERICAL RESULTS

From the numerical results, it was shown that the local Nusselt number, Nu_{local}, reached a steady-periodic state over a very short distance (Figure 2). This result is a fortunate occurrence in that most windows are analyzed from a one-dimensional centre-glass perspective, and ultimately a center-glass *U*-factor would be required for use in window rating software and building energy studies. As such, a center-glass Nusselt number, Nu_{cg}, was calculated at the center of the cavity between two consecutive louvers

$$Nu_{cg} = \frac{1}{2P}\int_{y_i}^{y_j} Nu_{local}\,dy \tag{2}$$

Nu_{local} is given by

$$Nu_{local} = \frac{q''W}{\Delta T k} \tag{3}$$

Here, k is the conductivity of the air, q'' is output by the software as $q''=-k\partial T/\partial x$ at the wall, and y_i and y_j are the vertical locations of consecutive slats.

Nu_{cg} is compared to the Rayleigh number in Figure 3 where Ra is given by

$$Ra = \frac{\rho^2 g\beta\Delta T W^3}{\mu^2}\Pr \tag{4}$$

where ρ, and μ are the density and dynamic viscosity, respectively. β is the volume expansion coefficient where $\beta = 1/T_{ref}$, and g is gravitational acceleration. Pr is the Prandtl number

$$Pr = \frac{\mu C_p}{k} \tag{5}$$

Here, C_p is the specific heat of the air. Fluid properties were evaluated at the reference temperature.

Figure 3 shows Nu_{cg} for all situations of θ_3= 0, 0.5, and 1, and on the right wall. As the system is symmetrical, Nu_{cg} at the left wall can be examined via the same plot where $\theta_{3,left} = |\theta_3 - 1|$ and the $Nu_{cg,left} = -Nu_{cg}$. For example, to examine Nu_{cg} on the left wall for $\theta_3=1$, then look at the results for $\theta_3=0$, and take the negative value of the resulting Nu_{cg}.

Examination of the numerical results suggested that a number of assumptions can be applied to the formulation of a simplified heat transfer model. These assumptions relate to the treatment of direct convection between the glass, the intra-louver heat transfer, and the glass-to-louver heat transfer characteristics.

- The energy transfer that would occur at the end regions, when the flow reverses cavity sides, and by air entrainment directly through the louvers, was found to be negligible.

From the numerical model, Nu_{local} was influenced at the ends of the cavity over a small distance, and therefore, the turn-around region is also small. Flow across the cavity was also negligible due to the formation of cells between the louvers. For these reasons, the convective heat transfer could be represented as the convective heat transfer from the glass-to-blind and blind-to-glass, without including a glass-to-glass term.

- Nu_{local} reached a steady-periodic state over a very short distance. Practically, this supports the one-dimensional centre-glass analysis preferred by building modelers.
- It was shown that the temperature drop across the cavity exists mostly between the blind tips and the glass. The convective cells that form between the slats create mixing which makes the blind-section of the cavity essentially isothermal (i.e., with negligible resistance to heat flow). Therefore, no resistance needs to be assigned to the blind section.
- The isotherms spread slightly into the spaces between the louvers. On the basis of this observation it seemed reasonable to treat convective heat transfer between the glass and the blind using established vertical cavity correlations, where the width of the cavity is based on the glass-to-blind spacing with some sort of geometric correction factor applied. That is *Ra* would be calculated on the basis of a cavity width which is a strong function of slat angle.

Combining these conclusions, the convective heat transfer in a window cavity with a blind can be treated as a combination of two vertical cavities from the glass-to-blind and blind-to-glass without accounting for the blind section. The cavity width will be some modified width based on the slat geometry and the slat tip-to-glass spacing.

CORRELATION DEVELOPMENT

Based on the previous analysis, it was decided that an attempt would be made to apply the vertical cavity correlation by Shewen et al. [11] to predict heat transfer in either side of the blind layer. The correlation is

$$Nu = \left[1 + \left(\frac{0.0665 Ra^{\frac{1}{3}}}{1 + \left(\frac{9000}{Ra} \right)^{1.4}} \right)^2 \right]^{\frac{1}{2}} \tag{6}$$

To do so, however, a fictitious cavity width, *L*, would need to be established which is comprised of the louver tip-to-glass spacing, *b*, plus a modifying distance, *c*, that

accounts for the fact that the flow on either side of the louver layer does broaden in the region between the louvers. Figure 4 shows the system and parameters under consideration. To further quantify the modifying distance, a fluid layer width modification factor, n^*, was also established where

. $$n^* = \left(1 - \frac{2c}{w\cos\phi}\right). \tag{7}$$

To find the parameter n^*, the following approach was established.

1. A half-cavity Rayleigh number, Ra', was calculated based on the estimated fictitious cavity width, L

$$Ra' = \frac{\rho^2 g\beta\Delta T' L^3}{\mu^2} Pr \tag{8}$$

where $\Delta T'$ is the temperature difference between the glass and the louvers, and the fluid properties were evaluated at the average of the glass and the louver temperature, T'_{ref}. Therefore,

on the right side cavity: $\Delta T' = (T_2 - T_3)$ $T'_{ref} = \frac{(T_2 + T_3)}{2}$

on the left side cavity: $\Delta T' = (T_1 - T_3)$ $T'_{ref} = \frac{(T_1 + T_3)}{2}$

2. The half-cavity Nusselt number, Nu', was calculated using Eqn. (6).
3. Recognizing that Nu' could also be represented by

$$Nu' = \frac{q''L}{\Delta T' k} \tag{9}$$

then

$$L = \frac{Nu'\Delta T' k_{@T'ref} W}{Nu_{cg}\Delta T k_{@Tref}} \tag{10}$$

Using the new value of L, repeat steps 1 through 3 until convergence.

4. When converged, c can be calculated using

$$c = L - \frac{W - w\cos\phi}{2} \tag{11}$$

and n^* is found using Eqn. (7)

Only the results for the 17.8 mm and 25.4 mm pane spacings were used in the aforementioned process. Results from the 40 mm pane spacing were excluded because it was thought that the Ra numbers were large enough to invalidate the laminar flow

assumption, and because that case represents a window which is rarely built due to structural limitations. Values of n^* are shown in Tables 3 to 5 for W=17.8mm and 25.4mm. θ_3=0 for the left side, and θ_3=1 for the right side have been omitted because there is no temperature difference between the glass and shade for those cases.

Using these results, an attempt was made to produce a correlation for n^*. Correlation tests, however, showed n^* was only weakly correlated to $cos\phi$, T_{ref}, and Ra. This was not surprising in that one of Huang's [6] conclusions was that, while n^* was important, it did not strongly influence the predicted convective heat transfer. As such, he found that setting n^* to a constant value of 0.70 produced excellent results unless the cavity spacing was wide. Following this conclusion, the average n^* value was found to be 0.61 with a standard deviation of ±0.04. Producing a weighted average, that increased the importance of n^* when the blinds were open and the cavity was narrow (i.e., small b), made no difference in the n^* constant quoted above.

COMPARISON TO HUANG [6]

As was previously mentioned, Huang [6] modeled the centre-glass U–factor using the concept of a thermal resistance network (Fig. 5). The convection model described in the previous section (using n^* = 0.70) was integrated with the radiation model developed by Yahoda and Wright [9], and used to simulate the glazing system samples tested in his experiments. Using this approach, he accurately reproduced experimentally determined U-factors.

It is useful to test the present constant in the same way. To use the correlation or constant presented, it is first necessary to determine the L

$$L = \frac{\left(W - n^* \times w\cos\phi\right)}{2} \tag{12}$$

Ra' is calculated using Eqn. (8) and Nu' is found using Equation (6). Finally, the convective heat transfer on each side of the cavity becomes

$$h_c = \frac{Nu'k}{L} \tag{13}$$

To remain consistent with the analysis of Huang [6], the combined radiative and convective heat transfer coefficient on the indoor and outdoor side of the window were 8 and 23 W/m^{2}K, respectively. The total thermal resistance of the glass layer, R_{glass}, was 0.006 m^{2}K/W. For a window containing a shading layer, the U-factor is given by [13]

$$U_{tot} = \left(R_{in\_2} + R_{1\_out} + R_{glass} + \frac{R_{1\_2}\left(R_{2\_3} + R_{3\_1}\right)}{R_{2\_1} + R_{2\_3} + R_{3\_1}} \right)^{-1} \tag{14}$$

where, $R = 1/(h_c+h_r)$. The techniques for solving the radiative heat transfer and for finding the radiative heat transfer coefficients for this model are discussed extensively in Yahoda and Wright [4], and Collins and Wright [12], respectively, and will not be reintroduced here.

The comparison between experimentally measured and predicted *U*-values are presented in Figure 6 and Table 6 for n^* values of 0.61, 0.70, and 1.00. Full details of the experimental parameters can be found in Huang [6]. In comparison to experimental results, an n^* of 0.61 predicts the *U*-factor with an average RMS error of 3.2% if the 40 mm results are excluded, and the maximum error is within 6% with one exception. Generally, the new constant is low in its prediction. Comparatively, results produced using n^*=0.70, as proposed by Huang [6], give the *U*-factor with an average RMS error of 1.5% with a maximum error within 3%. If no n^* constant is used (i.e., n^*=1.00), the RMS error is almost 10% irregardless of which spacings are considered, and the maximum error reached above 25% for a number of cases. Including the 40 mm cases, the average RMS errors are 6.6%, 5.0%, and 10.1% for n^* = 0.61, 0.70, and 1.00 respectively.

It is not surprising that the n^* value of 0.70 works better than the 0.61 value. Huang's constant was determined using his own experimental results and is therefore 'tuned' to the particular conditions of his tests. The value of n^*=0.61, however, was determined by an independent numerical study that, in difference to Huang's [6] experiments, had isothermal, flat, and curveless louvers, different glass and louver temperatures, and some different slat angles. It is surmised that, because of these differences, the value of n^* = 0.70 is still the better choice. The numerical model, however, as an approximation of the experimental setup, provide excellent confidence in the present approach in addition to insight into the flow structures occurring in the system.

CONCLUSIONS

Using numerical results, a cavity width modification factor of 0.61 was predicted for between-the-glass louvered shades, and a methodology is described for using this value to predict convective heat transfer within the glazing cavity. The convective predictions

were coupled with a longwave radiative model and compared to published experimental results.

The new value, while performing well, does not predict a system's *U*-factor better than the 0.70 value put forward by Huang [6]. Approximations made in the numerical model are likely the cause. It is suggested, therefore, that Huang's 0.70 value be used in practice. The numerical results do, however, provide confidence in the approach in addition to insight into the flow structures occurring in the system.

ACKNOWLEDGEMENTS

The Natural Sciences and Engineering Research Council of Canada and The CANMET Energy Technology Centre are gratefully acknowledged for their support of this work.

REFERENCES

[1] Garnet, J. M., Thermal performance of Windows with Inter-Pane Venetian Blinds, Ma.Sc Thesis, University of Waterloo, Waterloo, Ontario, Canada, 1999.

[2] Yahoda, S. D., Methods of Estimating the Effective Longwave and Solar Optical Properties of a Venetian Blind Layer for Use in Centre-Glass Glazing Analysis, Ma.Sc. Thesis, University of Waterloo, Waterloo, Ontario, Canada, 2002.

[3] Yahoda, S. D., and Wright, J. L., Methods for Calculating the Effective Longwave and Solar Optical Properties of a Venetian Blind Layer, ASHRAE Transactions, 110, part 1, 2004.

[4] Yahoda, S. D., and Wright, J. L., Heat Transfer Analysis of a Between-Panes Venetian Blind Using Effective Longwave Radiative Properties, ASHRAE Transactions, 110, part 1, 2004.

[5] Naylor, D., and Collins, M., Evaluation of an Approximate Method for Predicting the U-Value a Window with a Between-Panes Louvered Shade, Proceedings of CHT, 2004.

[6] Huang, N., Thermal performance of double glazed windows with inter-pane Venetian blinds, Ma.Sc. Thesis, University of Waterloo, Waterloo, Ontario, Canada, 2005.

[7] Tasnim, S., Collins, M., and Wright, J.L., Numerical Analysis of Convective Heat Transfer in Fenestration with Between-the-Glass Louvered Shades, Submitted to the International Journal of Heat and Mass Transfer, 2006.

[8] Hilsenrath, T., Thermal Properties of Gases, National Bureau of Standards Circular 564, 1955.

[9] Versteeg, H. K., Malalasekera, W., An introduction to Computational Fluid Dynamics, Prentice Hall, Pearson Education Limited, England, 1995.

[10] Ferziger, J., and Peric, M., Computational Methods for Fluids Dynamics 1st edition, Springer and Verlag, Berlin Hedelberg, 1996.

[11] Shewen, E. C., Hollands, K.G.T., Raithby, G.D., Heat Transfer by Natural Convection Across a Vertical Air Cavity of Large Aspect Ratio", J. Heat Transfer, Vol. 118, 1996, pp. 993–995.

[12] Collins, M., and Wright, J.L., Calculating Center-Glass Performance Indices of Windows with a Diathermanous Layer, ASHRAE Transactions, Vol. 112(2), 2006, pp. 22-29.

Table 1: Constant geometric parameters used in the numerical model

***H* (mm)**	***w* (mm)**	**No. of baffles**	**Pitch *P* (mm)**
367.0	14.8	30	11.8

Table 2: Input variables used in the numerical model

T_1(◦C)	T_2(◦C)	Θ_3	T_3(◦C)	ΔT(◦C)	W (mm)	ϕ (deg.)
-10.0	25.0	0.0	-10.0	35.0	17.8/25.4/40.0	-45, 0, 45
-10.0	25.0	0.5	7.5	35.0		
-10.0	25.0	1.0	25.0	35.0		
15.0	25.0	0.0	15.0	10.0		
15.0	25.0	0.5	20.0	10.0		
15.0	25.0	1.0	25.0	10.0		
40.0	25.0	0.0	32.5	-15.0		
40.0	25.0	0.5	25.0	-15.0		
40.0	25.0	1.0	25.0	-15.0		
-10.0	25.0	2.0	25.0	35.0	17.8/25.4	
15.0	25.0	4.0	25.0	10.0		
40.0	25.0	-1.0	40.0	-15.0		

Table 3: Values of n^* for ϕ=45°, W=17.78 mm and 25.4 mm. Nu' = 1 for all cases.

T_1 (°C)	T_2 (°C)	W (mm)	*Left Side*				*Right Side*			
			Θ_3	Nu_{cg}	Ra'	n^*	Θ_3	Nu_{cg}	Ra'	n^*
-10.0	25.0	0.0178	0.5	-1.66	366	0.69	0.5	1.66	324	0.63
15.0	25.0	0.0178	0.5	-1.55	100	0.60	0.5	1.55	97	0.58
40.0	25.0	0.0178	0.5	-1.55	119	0.57	0.5	1.55	124	0.60
-10.0	25.0	0.0178	1.0	-3.16	737	0.64	0.0	3.19	847	0.59
15.0	25.0	0.0178	1.0	-3.08	197	0.59	0.0	3.08	206	0.57
40.0	25.0	0.0178	1.0	-3.09	255	0.57	0.0	3.09	239	0.59
-10.0	25.0	0.0178	2.0	-6.44	1055	0.66	2.0	-3.12	519	0.56
15.0	25.0	0.0178	4.0	-12.51	595	0.60	4.0	-9.37	434	0.59
40.0	25.0	0.0178	-1.0	3.03	215	0.55	-1.0	6.22	416	0.60
-10.0	25.0	0.0254	0.5	-1.39	1845	0.71	0.5	1.39	1630	0.61
15.0	25.0	0.0254	0.5	-1.34	458	0.61	0.5	1.33	444	0.58
40.0	25.0	0.0254	0.5	-1.33	546	0.57	0.5	1.33	573	0.61
-10.0	25.0	0.0254	1.0	-2.77	3396	0.67	0.0	2.83	3867	0.59
15.0	25.0	0.0254	1.0	-2.66	893	0.60	0.0	2.66	934	0.57
40.0	25.0	0.0254	1.0	-2.66	1164	0.56	0.0	2.66	1089	0.60
-10.0	25.0	0.0254	2.0	-5.64	5870	0.59	2.0	-2.65	2512	0.52
15.0	25.0	0.0254	4.0	-10.98	2641	0.64	4.0	-8.03	2041	0.57
40.0	25.0	0.0254	-1.0	2.63	957	0.54	-1.0	5.39	1889	0.62

Table 4: Values of n^* for ϕ=0°, W=17.78 mm and 25.4 mm. Nu' = 1 for all cases.

T_1 (°C)	T_2 (°C)	W (mm)	*Left Side*				*Right Side*			
			Θ_3	Nu_{cg}	Ra'	n^*	Θ_3	Nu_{cg}	Ra'	n^*
-10.0	25.0	0.0178	0.5	-2.29	140	0.68	0.5	2.27	126	0.64
15.0	25.0	0.0178	0.5	-2.15	38	0.63	0.5	2.15	37	0.62
40.0	25.0	0.0178	0.5	-2.15	44	0.62	0.5	2.15	47	0.63
-10.0	25.0	0.0178	1.0	-4.57	243	0.68	0.0	4.66	271	0.66
15.0	25.0	0.0178	1.0	-4.23	76	0.62	0.0	4.23	79	0.61
40.0	25.0	0.0178	1.0	-4.26	97	0.61	0.0	4.25	92	0.63
-10.0	25.0	0.0178	2.0	-9.32	347	0.69	2.0	-4.07	234	0.58
15.0	25.0	0.0178	4.0	-17.25	227	0.63	4.0	-12.46	185	0.60
40.0	25.0	0.0178	-1.0	4.04	91	0.58	-1.0	8.53	161	0.63
-10.0	25.0	0.0254	0.5	-1.69	1016	0.72	0.5	1.69	903	0.66
15.0	25.0	0.0254	0.5	-1.59	273	0.63	0.5	1.59	264	0.61
40.0	25.0	0.0254	0.5	-1.59	320	0.61	0.5	1.59	335	0.64
-10.0	25.0	0.0254	1.0	-3.39	1760	0.72	0.0	3.45	1983	0.67
15.0	25.0	0.0254	1.0	-3.17	527	0.63	0.0	3.17	550	0.61
40.0	25.0	0.0254	1.0	-3.19	671	0.61	0.0	3.18	633	0.64
-10.0	25.0	0.0254	2.0	-7.05	2393	0.75	2.0	-3.17	1441	0.59
15.0	25.0	0.0254	4.0	-13.57	1363	0.70	4.0	-9.88	1083	0.65
40.0	25.0	0.0254	-1.0	3.11	579	0.58	-1.0	6.52	1055	0.66

Table 5: Values of n^* for ϕ=-45°, W=17.78 mm and 25.4 mm. Nu' = 1 for all cases.

T_1 (°C)	T_2 (°C)	W (mm)	*Left Side*				*Right Side*			
			Θ_3	Nu_{cg}	Ra'	n^*	Θ_3	Nu_{cg}	Ra'	n^*
-10.0	25.0	0.0178	0.5	-1.56	441	0.63	0.5	1.56	392	0.56
15.0	25.0	0.0178	0.5	-1.55	100	0.60	0.5	1.55	97	0.58
40.0	25.0	0.0178	0.5	-1.55	119	0.57	0.5	1.55	124	0.60
-10.0	25.0	0.0178	1.0	-3.16	738	0.64	0.0	3.08	940	0.55
15.0	25.0	0.0178	1.0	-3.08	196	0.59	0.0	3.08	205	0.57
40.0	25.0	0.0178	1.0	-3.09	255	0.57	0.0	3.18	219	0.63
-10.0	25.0	0.0178	2.0	-6.59	983	0.68	2.0	-3.11	522	0.56
15.0	25.0	0.0178	4.0	-12.70	569	0.62	4.0	-9.29	445	0.58
40.0	25.0	0.0178	-1.0	3.05	211	0.55	-1.0	6.19	422	0.60
-10.0	25.0	0.0254	0.5	-1.37	1917	0.69	0.5	1.37	1693	0.59
15.0	25.0	0.0254	0.5	-1.33	461	0.60	0.5	1.33	446	0.57
40.0	25.0	0.0254	0.5	-1.34	541	0.57	0.5	1.34	568	0.62
-10.0	25.0	0.0254	1.0	-2.76	3451	0.66	0.0	2.82	3905	0.59
15.0	25.0	0.0254	1.0	-2.66	895	0.60	0.0	2.66	938	0.57
40.0	25.0	0.0254	1.0	-2.67	1156	0.57	0.0	2.66	1084	0.61
-10.0	25.0	0.0254	2.0	-5.76	5153	0.67	2.0	-2.59	2728	0.46
15.0	25.0	0.0254	4.0	-11.14	2521	0.67	4.0	-8.10	1984	0.59
40.0	25.0	0.0254	-1.0	2.64	945	0.55	-1.0	5.36	1920	0.61

Table 6: Comparison of predicted versus experimental [8] U-factors. T_1 = 283 K and T_2 = 303 K in all cases[1].

Slat Angle	Glass[2]	W (mm)	U_{exper} (W/m^2K)	U_{celc} (W/m^2K) n*=0.61	Error	U_{celc} (W/m^2K) n*=0.70	Error	U_{celc} n*=1.00	Error
75	Cl-Cl	17.8	2.28	2.29	0.4%	2.32	1.8%	2.37	3.9%
60	Cl-Cl	17.8	2.50	2.48	0.8%	2.53	1.2%	2.66	6.4%
30	Cl-Cl	17.8	2.87	2.79	2.8%	2.89	0.7%	3.36	17.1%
0	Cl-Cl	17.8	3.08	2.91	5.5%	3.06	0.6%	3.85	25.0%
-30	Cl-Cl	17.8	2.86	2.79	2.4%	2.89	1.0%	3.36	17.5%
-60	Cl-Cl	17.8	2.54	2.48	2.4%	2.53	0.4%	2.66	4.7%
-75	Cl-Cl	17.8	2.32	2.29	1.3%	2.32	0.0%	2.37	2.2%
75	L□-Cl	17.8	1.84	1.83	0.5%	1.86	1.1%	1.93	4.9%
60	L□-Cl	17.8	2.00	1.98	1.0%	2.04	2.0%	2.22	11.0%
30	L□-Cl	17.8	2.38	2.27	4.6%	2.41	1.3%	3.04	27.7%
0	L□-Cl	17.8	2.65	2.40	9.4%	2.59	2.3%	3.63	37.0%
-30	L□-Cl	17.8	2.38	2.27	4.6%	2.41	1.3%	3.04	27.7%
-60	L□-Cl	17.8	2.02	1.98	2.0%	2.04	1.0%	2.22	9.9%
-75	L□-Cl	17.8	1.87	1.83	2.1%	1.86	0.5%	1.93	3.2%
75	Cl-Cl	25.4	2.21	2.08	5.9%	2.11	4.5%	2.13	3.6%
60	Cl-Cl	25.4	2.30	2.24	2.6%	2.27	1.3%	2.33	1.3%
30	Cl-Cl	25.4	2.54	2.47	2.8%	2.52	0.8%	2.66	4.7%
0	Cl-Cl	25.4	2.64	2.55	3.4%	2.61	1.1%	2.81	6.4%
-30	Cl-Cl	25.4	2.52	2.47	2.0%	2.52	0.0%	2.66	5.6%
-60	Cl-Cl	25.4	2.38	2.24	5.9%	2.27	4.6%	2.33	2.1%
-75	Cl-Cl	25.4	2.17	2.08	4.1%	2.11	2.8%	2.13	1.8%
75	L□-Cl	25.4	1.63	1.54	5.5%	1.56	4.3%	1.59	2.5%
60	L□-Cl	25.4	1.68	1.63	3.0%	1.66	1.2%	1.75	4.2%
30	L□-Cl	25.4	1.85	1.78	3.8%	1.84	0.5%	2.07	11.9%
0	L□-Cl	25.4	1.94	1.84	5.2%	1.92	1.0%	2.23	14.9%
-30	L□-Cl	25.4	1.87	1.78	4.8%	1.84	1.6%	2.07	10.7%
-60	L□-Cl	25.4	1.84	1.63	11.4%	1.66	9.8%	1.75	4.9%
-75	L□-Cl	25.4	1.65	1.54	6.7%	1.56	5.5%	1.59	3.6%
75	Cl-Cl	40.0	2.20	1.92	12.7%	1.95	11.4%	1.95	11.4%
60	Cl-Cl	40.0	2.35	2.05	12.8%	2.08	11.5%	2.10	10.6%
30	Cl-Cl	40.0	2.47	2.24	9.3%	2.28	7.7%	2.32	6.1%
0	Cl-Cl	40.0	2.49	2.31	7.2%	2.34	6.0%	2.39	4.0%
-30	Cl-Cl	40.0	2.43	2.24	7.8%	2.28	6.2%	2.32	4.5%
-60	Cl-Cl	40.0	2.27	2.05	9.7%	2.08	8.4%	2.10	7.5%
-75	C-C	40.0	2.14	1.92	10.3%	1.95	8.9%	1.95	8.9%
75	L□-Cl	40.0	1.78	1.31	26.4%	1.34	24.7%	1.35	24.2%
60	L□-Cl	40.0	1.82	1.36	25.3%	1.38	24.2%	1.40	23.1%
30	L□-Cl	40.0	1.81	1.42	21.5%	1.45	19.9%	1.51	16.6%
0	L□-Cl	40.0	1.76	1.44	18.2%	1.48	15.9%	1.56	11.4%
-30	L□-Cl	40.0	1.73	1.42	17.9%	1.45	16.2%	1.51	12.7%
-60	L□-Cl	40.0	1.74	1.36	21.8%	1.38	20.7%	1.40	19.5%
-75	L□-Cl	40.0	1.78	1.31	26.4%	1.34	24.7%	1.35	24.2%

[1] Huang also presented results for $T_1 = 293$. These results were included in Figure 6, but have been excluded from the Table for brevity. In all cases, the different temperature resulted in less that a 2% difference in the measured *U*-factor.
[2] Cl-Cl is Clear glass on both sides. Lowε-Cl has a low-ε coating (ε = 0.164) on the outdoor glass.

Figures

Figure 1: System geometry and computational domain.

Figure 2: Variation of Nu_{local} along the right wall of the cavity for W=17.8mm, ϕ=0^0, T_1=15^0C, and T_2=25^0C. For left wall: $\theta_{3,left} = |\theta_3 - 1|$ and $Nu_{local,left} = -Nu_{local}$.

Figure 3: Nu_{cg} for ϕ=45^o (top), ϕ=0^o (mid), and ϕ=-45^o (bottom) on the right wall. For left wall: $\theta_{3,left} = |\theta_3 - 1|$ and $Nu_{cg,left} = -Nu_{cg}$. Only θ_3=0, 0.5, and 1 plotted.

Figure 4: Parameters used in correlation development.

Figure 5: Thermal resistance network for a typical window where the centre glazing is a diathermanous layer.

Figure 6: Experimental versus predicted U-factors for different values of n^*. Measured values have been obtained from Huang [6].

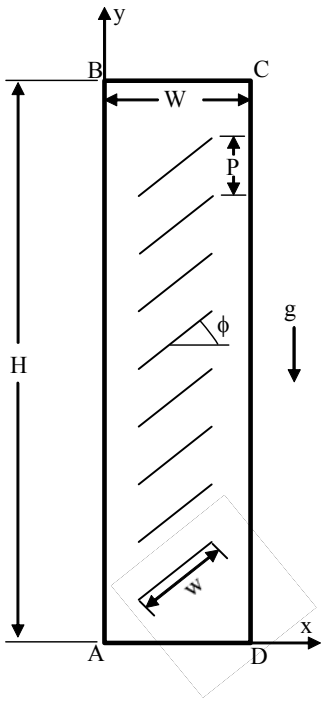

Figure 1: System geometry and computational domain.

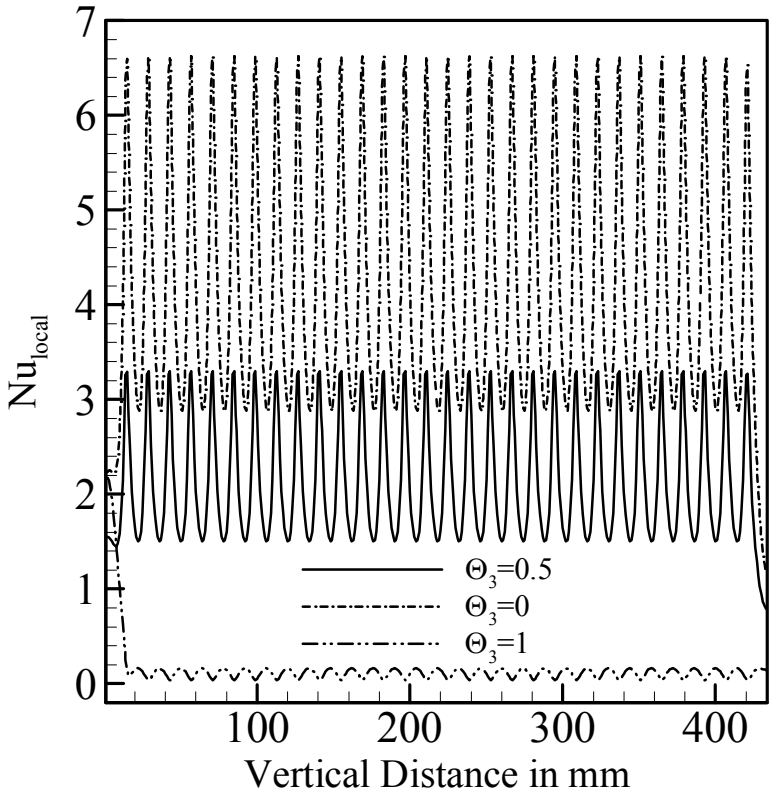

Figure 2: Variation of Nu_{local} along the right wall of the cavity for W=17.8mm, ϕ=0^0, T_1=15^0C, and T_2=25^0C. For left wall: $\theta_{3,left} = |\theta_3 - 1|$ and $Nu_{local,left} = -Nu_{local}$.

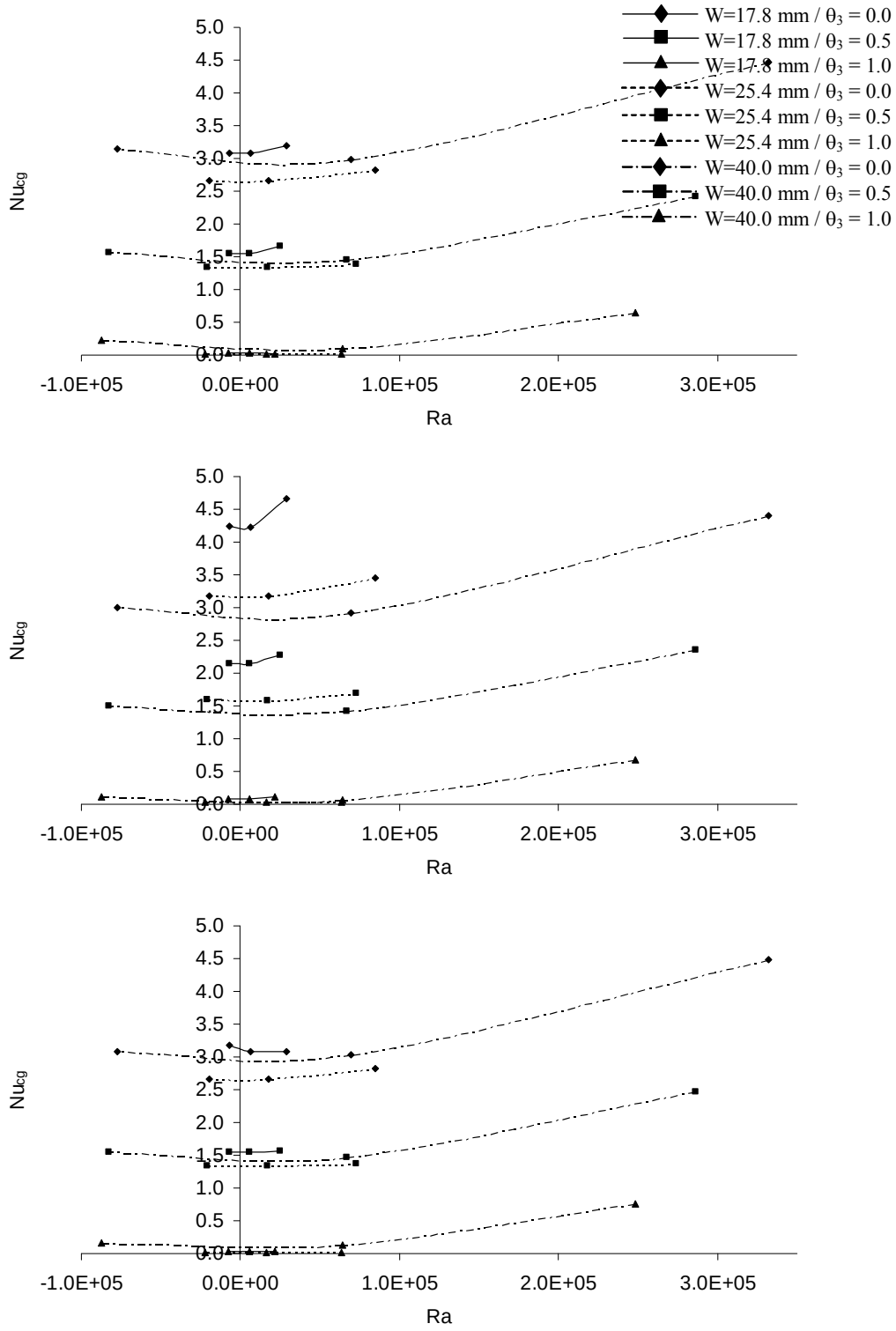

Figure 3: Nu_{cg} for ϕ=45° (top), ϕ=0° (mid), and ϕ=-45° (bottom) on the right wall. For left wall: $\theta_{3,left} = |\theta_3 - 1|$ and $Nu_{cg,left} = -Nu_{cg}$. Only θ_3=0, 0.5, and 1 plotted.

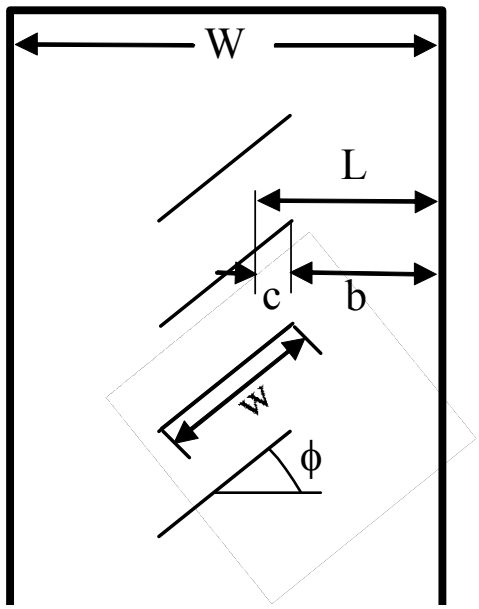

Figure 4: Parameters used in correlation development.

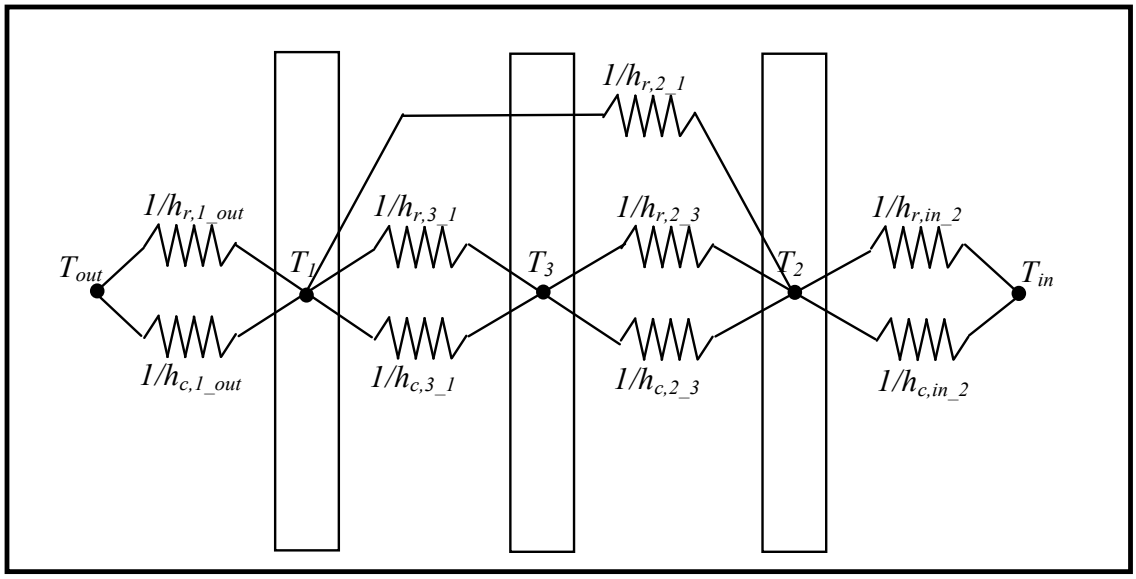

Figure 5: Thermal resistance network for a typical window where the centre glazing is a diathermanous layer.

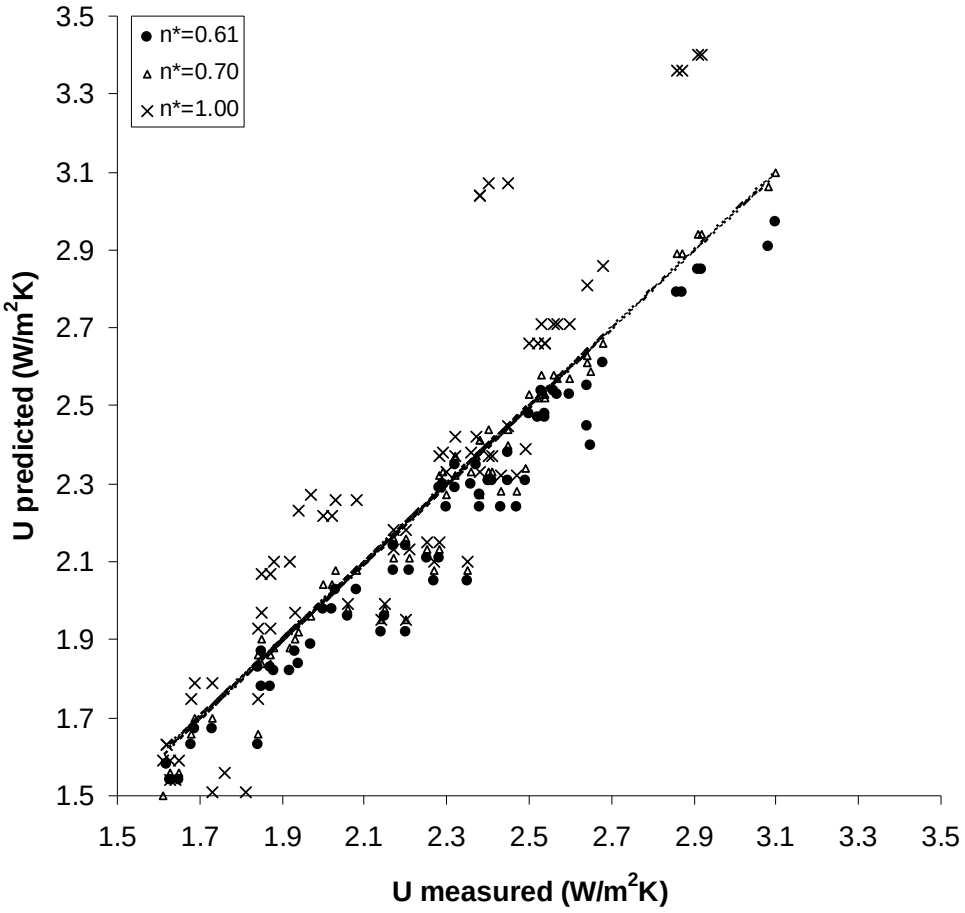

Figure 6: Experimental versus predicted U-factors for different values of n^*. Measured values have been obtained from Huang [6].